ISSN 0869-5911, Petrology, 2006, Vol. 14, No. 3, pp. 209–229. © Pleiades Publishing, Inc., 2006.
Original Russian Text © L.V. Dmitriev, S.Yu. Sokolov, A.A. Plechova, 2006, published in Petrologiya, 2006, Vol. 14, No. 3, pp. 227–247.

Statistical Assessment of Variations in the Compositional and *P–T* Parameters of the Evolution of Mid-Oceanic Ridge Basalts and Their Regional Distribution

L. V. Dmitriev[a]†, S. Yu. Sokolov[b], and A. A. Plechova[a]

[a] *Vernadsky Institute of Geochemistry and Analytical Chemistry, Russian Academy of Sciences, ul. Kosygina 19, Moscow, 119991 Russia*
e-mail: ldmitr@geokhi.ru, aplech@geokhi.ru

[b] *Geological Institute, Russian Academy of Sciences, Pyzhevskii per. 7, Moscow, 109017 Russia*
e-mail: geophys@ginras.ru

Received January 20, 2005

Abstract—The formal statistical analysis of variations in the basalt compositions for the whole global system of mid-oceanic ridges (approximately 19000 analyses of quenched glasses), including cluster analysis, discriminant analysis, and the analysis of histograms and component covariations, provide new data on the petrological parameters of the evolution of mantle magmatism and the spatial distribution of its products depending on geodynamic environments. The results thus obtained make it possible to assess all available information on magmatism in mid-oceanic ridges and to specify tasks for the further research. The information thus obtained is required for the development of the petrological basis for a model of magmatism of six major basalt groups (*P–T* parameters, productivity of volcanism, mantle upwelling, etc.).

DOI: 10.1134/S0869591106030015

INTRODUCTION

Basalts of mid-oceanic ridges (MORB and TOR[1] are the products of mantle volcanic activity in the oceanic segments of the Earth that occur as flows of pillow lavas along the axes and flanks of the rift zones of mid-oceanic ridges. Now extensive information is accumulated on their petrography, mineralogy, petrochemistry, geochemistry, relations between geologic structures, etc. At the same time, a wide circle of problems concerning relations between oceanic magmatism and the deep mantle structure and geodynamics remains unsettled as of yet.

The compositional variations of mid-oceanic ridge basalts provide insight into their genesis, which is crucial for understanding the origin and evolution of the oceanic lithosphere. This research is continuously conducted based on the results of petrological experiments and data on the trace-element and isotopic geochemistry of these rocks. Recent publications present newly obtained important and comprehensive information concerning this problem and deserve worldwide recognition. However, the accumulation of factual material on the composition of basalts in individual geologic structures and with reference to geophysical fields, considered in the context of relations between petrological and geophysical parameters, highlights the need to refine certain data obtained in the course of earlier studies. In this context, it was required to refine and systematize information on the variations in the petrochemistry of basalts sampled throughout the whole world's system of mid-oceanic ridges without reference to the broadly known information on their petrography and mineralogy.

One of our earlier publications statistically justified the classification of TOR in the northern segment of the Mid-Atlantic Ridge (MAR) (Dmitriev et al., 1990). The factual materials were based on the catalogue of the compositions of quenched TOR glasses published by the Smithsonian Institution (Melson et al., 1977), which was supplemented with data from later publications (5882 microprobe analyses). The cluster analysis of this material made it possible to distinguish six TOR groups with different character of their compositional variations and the petrological parameters of their evolution. The first four groups (TOR-1, TOR-2, TOR-Na, and TOR-K) are the differentiation products of four different parental melts that are generated in the mantle at different depths, temperatures, and degrees of melting. TOR-1 and TOR-2 compose the background of all volcanism and quantitatively dominate in mid-oceanic ridges. The parental melts of TOR-1 are derived in the mantle at greater depths and at higher temperatures and degrees of melting than those of TOR-2. The petrological parameters of TOR-1 and TOR-2 evolution were

† Deceased.

[1] TOR, the abbreviation for the tholeiites of oceanic rifts, was proposed (Dmitriev et al., 1978) as an alternative to MORB.

determined experimentally. TOR-Na are the differentiation products of melts produced in the mantle at shallow depths and at the lowest degrees of melting, temperatures, and pressures. These rocks occur locally. The petrological parameters of the evolution of TOR-Na were determined by calculations. TOR-K are produced by the deepest mantle magmatism in the system of mid-oceanic ridges, and the nature and characteristics of these rocks are transitional to those of the products of oceanic-island magmatism (OIB). TOR-1 and TOR-K are members of the plume association of basalts, and TOR-2 and TOR-Na belong to the spreading-related association. It was established that Ti, Na, and K are indicator elements of spreading and plume TOR associations: spreading associations are enriched in TiO_2 and Na_2O, whereas plume associations contain relatively much K_2O. The remaining two groups, TOR-Fe and TOR-FeTi, are produced by the differentiation of TOR-1 and TOR-2, respectively, in magmatic chambers. The distribution of these six groups in MAR was determined statistically and displayed in the petrological map of the Atlantic Ocean published in (Dmitriev et al., 1990).

Later, with the further amassing of factual materials, the same six groups of TOR were identified in the East Pacific Rise (EPR), and their composition and spatial distribution were examined in detail. The groups were identified without cluster analysis, based only on the average compositions and standard deviations calculated previously for the northern part of MAR. In the course of this research, we have determined the affiliation of the groups with spreading or plume basalt associations and clarified their relations to the deep structure of the mantle and geodynamic characteristics of the development of mid-oceanic ridges with various spreading velocities (Dmitriev, 1998; Dmitriev et al., 1999, 2002; Dmitriev and Sokolov, 2003).

This study is a continuation of our earlier research and involves the detailed examination of correlations between the geophysical and petrological parameters of the origin of the oceanic lithosphere on the basis of modern data. In this context, it seems to be expedient to refine the compositional variations of the six TOR groups based on all data on the ocean as a whole with the use of formalized statistical approaches.

FACTUAL MATERIAL

The basis of the databank of the compositions of TOR quenched glasses used in this research, which was conducted at the Vernadsky Institute of Geochemistry and Analytical Chemistry, Russian Academy of Sciences, is the new Smithsonian Volcanic Glass Data File (*Smithsonian…*, 2000) and a database of petrological information of the Lamont-Doherty Earth Observatory of the Columbia University (*Ridge…*, 1999). This material was supplemented with original data obtained by the authors and with literature information published in the past years. The database comprises 18793 microprobe analyses with analytical totals for major elements of 100 ± 1.5%, calibrated on the M 111 240/52 standard (Jarosevich et al., 1979).

STATISTICAL ANALYSIS OF VARIATIONS IN THE COMPOSITIONS AND PETROLOGICAL PARAMETERS

Figure 1 displays a SiO_2–($Na_2O + K_2O$) diagram for the variations in the compositions of seafloor volcanic rocks that were included in the database of the Vernadsky Institute. This diagram is still successively used to the simplified systematics of magmatic rocks (McDonald and Katsura, 1962).

According to the currently adopted nomenclature, rocks with $SiO_2 > 53$ wt % are classed with intermediate and acid varieties. They can be regarded as the products of the deep differentiation of basalts. Rocks with ($Na_2O + K_2O$) > 5 wt % are ascribed to subalkaline and alkaline basaltoids, which are possible products of within-plate magmatism. The former rocks are represented by 476 analyses, which makes up 2.5% of all analyses composing the database. These rocks occur predominantly in structures adjacent to the system of island arcs and islands in the Pacific Ocean. They were found in MAR near Iceland, at the Azores plume, and in Ascension Island.

Rocks of elevated alkalinity are represented by 238 analyses (1.3% of the database). They occasionally occur in areas adjacent to islands of the Pacific seafloor and in the vicinity of the Azores plume and Iceland. These rocks (referred to as acid and subalkaline) are not discussed in this publication.

Statistical analysis was conducted for tholeiitic basalt (TOR) whose compositions cluster within a compact field (core) in the SiO_2–($Na_2O + K_2O$) diagram (Fig. 1) and are represented by 18 079 analyses.

As was mentioned above, cluster analysis of a limited selection of data (5882 analyses) has revealed six stable TOR groups. This publication presents the results of the cluster analysis of the compositional variations of TOR for the whole system of mid-oceanic ridges on the basis of all available data (18079 microprobe analyses of quenched glasses).

The cluster analysis routine was conducted in a number of stages, with the use of additional information, which was obtained from the data of histograms and variation diagrams for key components.

Clusters were calculated for five variants of the sets of arguments that persistently determine the maximum differences between the compositions:

(1) all eight major components: SiO_2–TiO_2–Al_2O_3–FeO–MgO–CaO–Na_2O–K_2O;

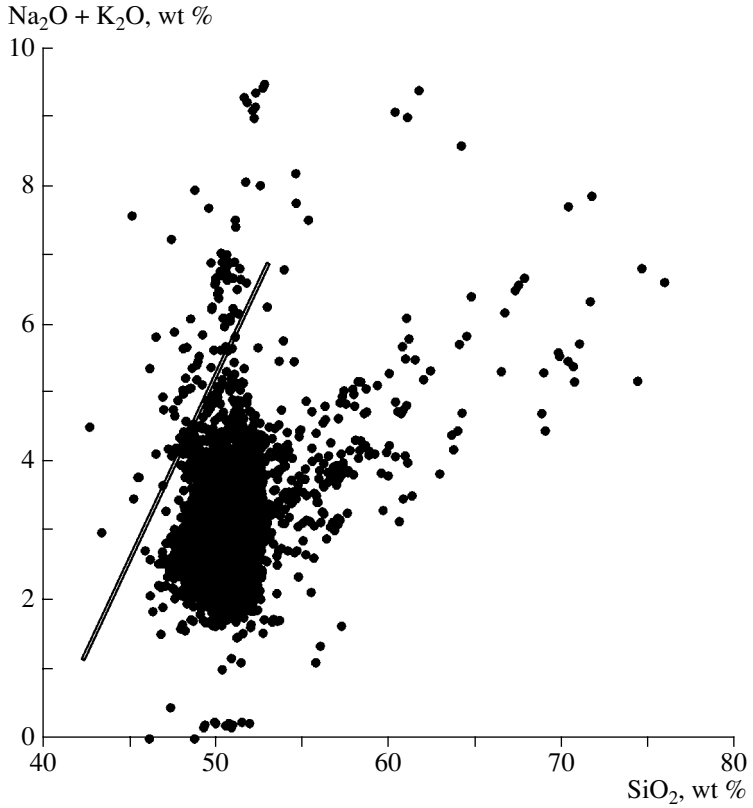

Fig. 1. SiO_2–($Na_2O + K_2O$) diagram (McDonald and Katsura, 1962) for the composition of volcanic rocks from the seafloor. The slant line separates the alkaline and tholeiitic series.

(2) four components with the maximum dispersion of concentrations: TiO_2–FeO–Na_2O–K_2O;

(3) the same four components and the Na_2O/MgO ratio (the degree of melting divided by the degree of differentiation);

(4) the K_2O/TiO_2 ratio (degree of enrichment)–Na_2O/MgO (the degree of melting divided by the degree of differentiation)–FeO/MgO (Fe#);

(5) three components with the maximum dispersion TiO_2–Na_2O–K_2O and the K_2O/TiO_2 and Na_2O/MgO ratios.

Each set of the arguments was treated by cluster analysis using the STATISTICA software package for data analysis with the preliminary standardization of the variables (which were brought to zero means and unit variances). The data table whose rows were individual analyses and the columns were the arguments was processed by STATISTICA to calculate the subdivision of the whole body of analyses into subgroups by the K-means clustering procedure. The latter technique makes use of the outlining of isolated subsets in an *n*-dimension space, where *n* is the number of the arguments. This process is conducted as follows. The classification algorithm is specified by a certain starting radius *r* in dimensionless (because of standardization) coordinates, with *r* being so small that spheres of radius *r* drawn around each point are not intersected. As the radius is increased, the elementary spheres begin merging into variable volumes that outline data subsets. The process is aborted when the number of the subsets becomes equal to the desired number of clusters. The output of the procedure provides coordinates for the centers of the cluster subsets, their average radii, and a table with the affiliation of each analysis with a cluster of certain number. Theoretically, this procedure can be implemented in the reverse sequence of the change in the radius of the sphere, i.e., from an originally large radius *r* that comprises all points toward its smaller values. The original hypersphere is then subdivided into smaller volumes until the desired number of clusters is achieved. The calculation routine in STATISTICA also involves some technicalities that will be not discussed in this publication.

The most important issue in the calculation method is the selection of the "right" number of clusters to subdivide the analytical data set. This number is specified by the researcher based exclusively on the expedience and appropriateness of the desired classification. In order to determine the optimum number of the clusters, a series of calculation iterations (steps) should be conducted with a gradual increase in the number of the final clusters from an apparently minimum value (for example, 2) to a value apparently exceeding the physically achievable and instrumentally distinguishable

diversity of the groups. The optimum number of clusters should occur somewhere in between and can be determined using the following asymptotic criteria. Assume that the calculations of the clusters are conducted with the subdivision of the set of clusters with a step for two to ten clusters. Inasmuch as two target clusters obviously do not describe the whole diversity of the groups, we proceed to the next step of three clusters. This usually results in the distinguishing of a new group with notably different parameters, and so on. If the increase in the number of clusters at each step leads to a value exceeding the physically justified optimum and the number of clusters tends to infinity (i.e., to the original number of analyses), the calculations result in clusters virtually indistinguishable from one another, whose parameters vary around the mean values. This increasing concentration of cluster parameters within some small value relative to the mean values indicates that the optimum was missed during the execution of the calculation steps, and the algorithm is forced to continue classifying where this is unreasonable. Hence, the optimum number of clusters is equal to a value at which pervasively different groups of clusters end to form, and the cluster parameters start to "swarm" around the mean values and range within the instrumental accuracy.

All variants starting at step 4 (4 clusters each) display similarities between the groups of the compositional variations with one another and with the compositional fields of TOR-1, TOR-2, TOR-Na, and TOR-K determined previously.[2] They differed only in the location of the boundaries between the compositional fields and the extent of their overlaps. The maximum similarities between the fields of TOR and those determined in the calculations were achieved during step 4 of the fifth set of components (three components with the maximum dispersion TiO_2–Na_2O–K_2O and the K_2O/TiO_2 and Na_2O/MgO ratios). This is clearly seen in Fig. 2, which presents a Na_2O/MgO vs. K_2O/TiO_2 diagram for the compositional fields of TOR determined by calculating the clusters of variant 5 (Fig. 2a) and corresponding fields established previously (Fig. 2b; Dmitriev and Sokolov, 2003). Note that none of the cluster analysis variants managed to distinguish compositional fields corresponding to TOR-Fe and TOR-FeTi. This can be explained by the fact that both of these groups have relatively insignificant volumes and are the differentiation products of TOR-1 and TOR-2. During our earlier research, the compositions attributed to ferrous basalts had more than 12 wt % FeO, and they were subdivided into TOR-Fe and TOR-FeTi by analyzing some variation diagrams (Dmitriev and Sokolov, 2003).

Having generally similar configurations of their compositional fields, the diagrams in Figs. 2a and 2b exhibit certain differences. This can be explained by the fact that cluster analysis was previously applied only to the northern MAR segment but not to the whole ocean. To clarify how stable are the compositional variations of TOR-1, TOR-2, TOR-Na, and TOR-K and also to outline the compositional fields of TOR-Fe and TOR-FeTi, we examined and used the data of histograms for FeO, Na_2O, K_2O, and K_2O/TiO_2 for all data from the database and for each of the four clusters of variant 5.

Statistically significant maxima in the K_2O concentrations (0.25 wt %) and the K_2O/TiO_2 ratio (0.2–0.3) were identified in all clusters. This led us to notably expand the compositional field of cluster 5_4_1, corresponding to TOR-K, at the expense of other fields.

The weakly pronounced minimum at 2.5–3 wt % Na_2O can be seen in the histogram for the whole database. It corresponds to the compositional gap at ~2.8 wt % Na_2O in the MgO–Na_2O diagram for cluster 5_4_3, corresponding to TOR-Na.

In the histogram for Na_2O, this cluster also displays a weak minimum at 2.8 wt % Na_2O. This provided grounds to exclude compositions with $Na_2O < 2.8$ wt % from the cluster corresponding to TOR-Na.

Two notable minima in the FeO concentrations (at 11.5 and 13 wt %) can be seen in the histogram for the whole database. The minimum at 11.5 wt % is clearly pronounced in the histogram of cluster 5_4_4, which corresponds to TOR-1, and the minimum at 13 wt % is seen in the histogram for 5_4_2, corresponding to TOR-2. This led us to exclude compositions with FeO > 13 wt %, which were then combined into the group of TOR-FeTi. Compositions with FeO > 11.5 wt % were combined in the group of TOR-Fe.

The compositions of clusters 5_4_4 and 5_4_2, after the excluding of compositions corresponding to TOR-Fe and TOR-FeTi from them, along with compositions with $K_2O > 0.25$ wt % and with $Na_2O > 2.8$ wt %, can be regarded as TOR-1 and TOR-2, respectively.

Figure 3 presents a Na_2O/MgO–K_2O/TiO_2 diagram for all compositions of the six TOR groups calculated by the aforementioned procedure. This diagram can be used to identify various TOR groups by newly obtained materials.

Table 1 summarizes all information on the average compositions and standard deviations for the whole body of data on the ocean and for all TOR groups obtained in our research. For comparison, this table also presents the data from (Dmitriev and Sokolov, 2003).

The analysis of the materials reported in Table 1 demonstrates the following.

After the publication of (Dmitriev and Sokolov, 2003), the databank was supplemented with a selection of only 267 analyses, and hence, the average compositions of oceanic basalts remained practically unchanged.

[2] The compositional fields appearing during calculation steps 5, 6, and 7 significantly overlap.

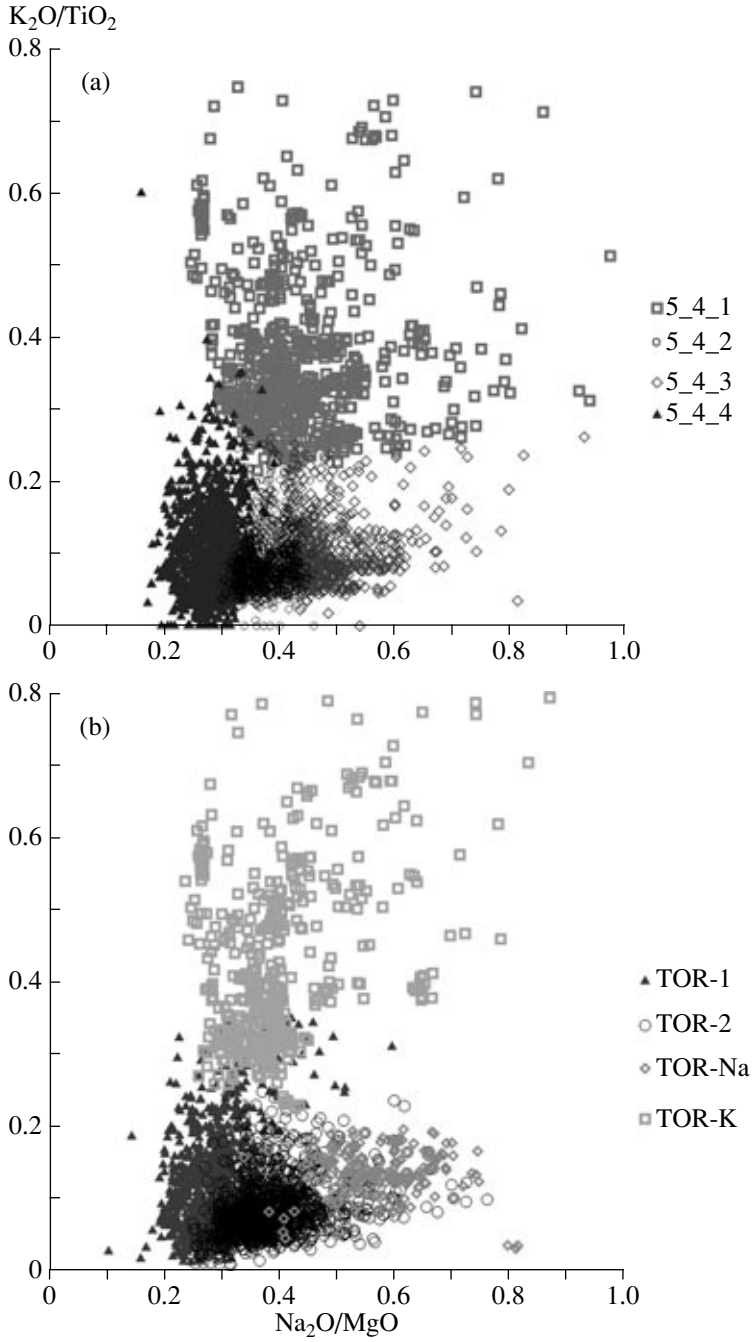

Fig. 2. Compositional fields of TOR calculated in (a) (Dmitriev and Sokolov, 2003) and (b) this paper. The compared fields are shown by analogous symbols.

The proportions of plume and spreading basalt associations were also virtually not changed: 32 and 68% in 2003 and 33 and 67% according to the results of the newly conducted calculations.

Notable changes were caused by the redistribution of the percentages of various TOR groups. The percentage of TOR-1 in the plume association has decreased (20 against 33%) because of an increase in the percentage of TOR-K (11 against 1%), and the percentage of TOR-Fe has doubled (2 instead of 1%). In the spreading association, the percentage of TOR-2 has decreased from 61 to 57%, and the percentages of TOR-Na and TOR-FeTi have notably increased (5 instead 2% and 4 instead 2%, respectively).

Some changes also occurred with the average compositions of various TOR groups. The most remarkable of them are an increase in the Mg# of TOR-1, TOR-Fe, and TOR-FeTi, an increase in the Na_2O and TiO_2 con-

Table 1. Average compositions (*X*, wt %) and standard deviations (σ) of basalts from mid-oceanic ridges of the plume and spreading associations

Component	MOR basalts		Plume association						Spreading association					
			TOR-1		TOR-K		TOR-Fe		TOR-2		TOR-Na		TOR-FeTi	
	X	σ	*X*	σ	*X*	σ	*X*	σ	*X*	σ	*X*	σ	*X*	σ
Data from this publication														
SiO_2	50.85	0.80	50.80	0.86	51.18	1.10	51.07	0.57	50.78	0.70	51.15	0.77	50.93	0.76
TiO_2	1.54	0.42	1.08	0.18	1.68	0.46	1.36	0.19	1.57	0.28	2.11	0.26	2.41	0.46
Al_2O_3	15.20	1.00	15.52	0.78	15.83	1.09	14.15	0.41	15.20	0.88	14.85	0.92	13.21	0.64
FeO	10.25	1.42	9.53	0.77	9.44	1.31	12.33	0.42	10.22	1.07	11.01	1.28	14.20	1.17
MgO	7.50	0.88	8.29	0.69	6.98	0.92	7.07	0.39	7.57	0.64	6.48	0.50	5.77	0.54
CaO	11.65	0.79	12.39	0.51	11.20	1.01	11.76	0.38	11.66	0.55	10.64	0.67	10.35	0.63
Na_2O	2.66	0.41	2.18	0.19	2.89	0.48	2.06	0.12	2.74	0.26	3.33	0.31	2.75	0.36
K_2O	0.18	0.16	0.12	0.06	0.56	0.24	0.11	0.05	0.13	0.06	0.24	0.07	0.18	0.06
K_2O/TiO_2	0.11	0.09	0.11	0.05	0.33	0.11	0.08	0.03	0.08	0.04	0.12	0.04	0.07	0.03
N	18079		3648		1941.0		428		10346		1002.0		714	
%	100		20.18		10.74		2.37		57.22		5.54		3.95	
(Dmitriev and Sokolov, 2003)														
SiO_2	50.86	0.81	50.97	0.94	50.28	1.09	53.36	3.03	50.80	0.72	50.67	0.83	52.68	3.21
TiO_2	1.54	0.43	1.28	0.35	1.57	0.32	1.96	0.58	1.69	0.40	1.61	0.23	2.84	0.67
Al_2O_3	15.21	1.01	15.23	1.01	16.38	0.79	13.38	1.26	15.20	1.02	16.14	0.84	12.83	1.75
FeO	10.26	1.43	10.17	1.47	8.60	1.34	13.91	2.15	10.31	1.41	9.22	0.81	14.78	2.27
MgO	7.50	0.89	7.72	0.95	7.69	0.57	3.57	1.16	7.38	0.84	7.65	0.48	4.22	1.12
CaO	11.65	0.82	12.02	0.85	11.73	1.59	8.16	1.18	11.45	0.73	11.00	0.83	8.71	1.20
Na_2O	2.66	0.42	2.28	0.32	2.64	0.48	2.85	0.37	2.86	0.32	3.40	0.20	3.22	0.54
K_2O	0.19	0.20	0.22	0.28	0.87	0.53	0.49	0.26	0.17	0.14	0.18	0.06	0.38	0.26
K_2O/TiO_2	0.12	0.13	0.16	0.19	0.57	0.40	0.28	0.20	0.10	0.07	0.11	0.04	0.60	0.09
N	17812		5812		216		184		10834		325		441	
%	100		32.6		1.21		1.03		60.82		1.82		2.47	

Note: *N* is the number of analyses in each group and their percentage of the whole data body.

tents in TOR-K and TOR-Na, and a decrease in the Na_2O and TiO_2 concentrations in TOR-1, TOR-Fe, and TOR-FeTi. The average composition of TOR-Na became somewhat richer in TiO_2, FeO, and K_2O, while the average composition of TOR-2 remained practically unchanged.

These changes are explained by the fact that the application of cluster analysis of key components to the whole body of data (18 079 analyses instead of 5882) made it possible to determine more accurately the variations in the compositions of basalts, distinctive features of their differentiation, and affiliation with certain groups. The changes in the compositional variations were also affected by some regional features in the distribution of various TOR groups. The compositional variations of individual TOR groups are illustrated in a series of diagrams presented below (to simplify the reading of these diagrams, symbols are plotted in them with different intervals and with steps from 1 to 30 depending on the volumes of discrete compositional groups).

The MgO–FeO diagram in Fig. 4 demonstrates that the compositions of the most widely spread groups TOR-1 and TOR-2 plot differently, and their fractionation trends have different slopes. This confirms our earlier conclusion that the differentiation products of

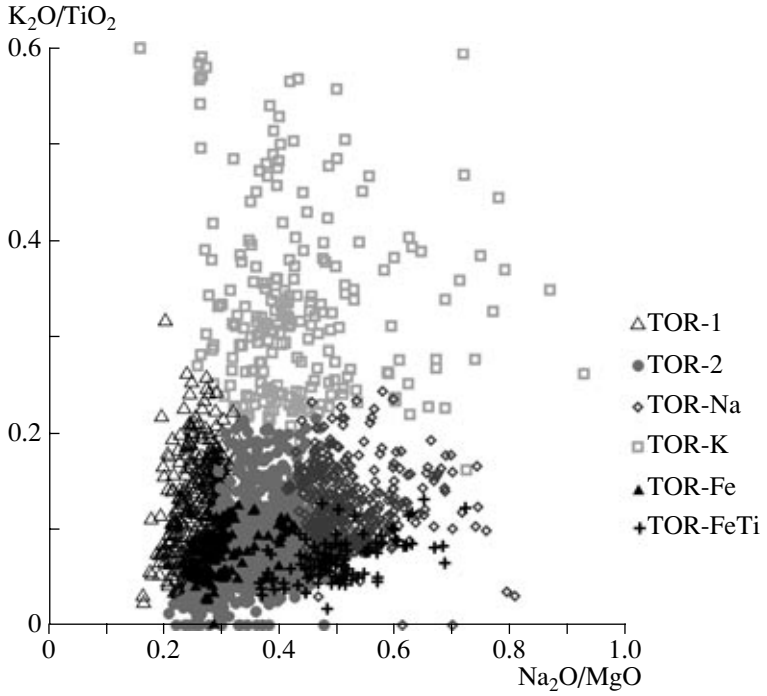

Fig. 3. $Na_2O/MgO–K_2O/TiO_2$ diagram for the composition of TOR of the World Ocean based on the results of cluster analysis (arguments: $TiO_2–Na_2O–K_2O–K_2O/TiO_2–Na_2O/TiO_2$) with regard for the data of histograms (see text).

these groups have distinct mantle sources: that of TOR-1 is deeper sitting and higher temperature (magnesian) than the source of TOR-2.

Figures 5, 6, and 7 illustrate the differences between the fractionation trends of indicator elements (TiO_2 and Na_2O) and the K_2O/TiO_2 ratio for the major groups of TOR-1, TOR-2, TOR-Na, and TOR-K. It can be easily seen that the differentiation of TOR-2 and TOR-Na is associated with a more rapid increase in the concentrations of TiO_2 than those for TOR-1 (Fig. 5), a feature explaining the elevated TiO_2 concentrations in the basalts of the spreading association. Figure 6 clearly demonstrates the two levels of the Na_2O concentrations in the major groups of TOR-1 and TOR-2: it is the highest in TOR-Na and possibly decreases during the fractionation of TOR-Na.

This definitely testifies that the mantle source of the basalts of the spreading association is enriched in Na_2O relative to the basalts of plume association. Figure 7 demonstrates parallel enrichment trends for TOR-1 and TOR-2, with the trend for TOR-1 situated above the trend for TOR-2. The close spacing of the trends explains the similarities between the K_2O/TiO_2 ratios for the intermediate compositions of both groups and corroborates the earlier conclusion that the parental melts of TOR-1 (plume association) are enriched more strongly than those of TOR-2 (spreading association).

The behavior of Na_2O and TiO_2 during the differentiation of TOR-K is the same as in the other major groups. At the same time, Figs. 5, 6, and 7 demonstrate

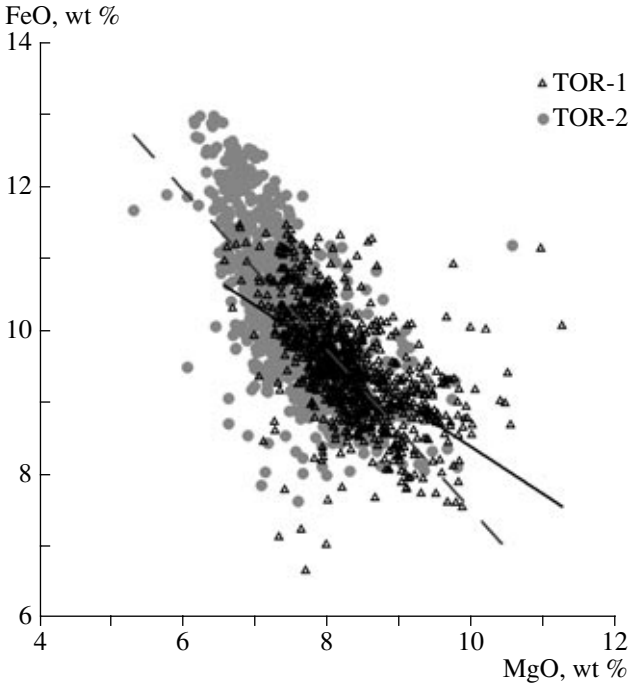

Fig. 4. MgO–FeO diagram for the composition of TOR-1 and TOR-2. The different slopes of the differentiation trends of TOR-1 and TOR-2 suggest that these two groups could have been derived from different mantle sources. The lower angle between the TOR-1 differentiation trend solid line and the MgO axis than that of the TOR-2 trend (dashed line) testifies to the higher Mg# of the parental melts of TOR-1.

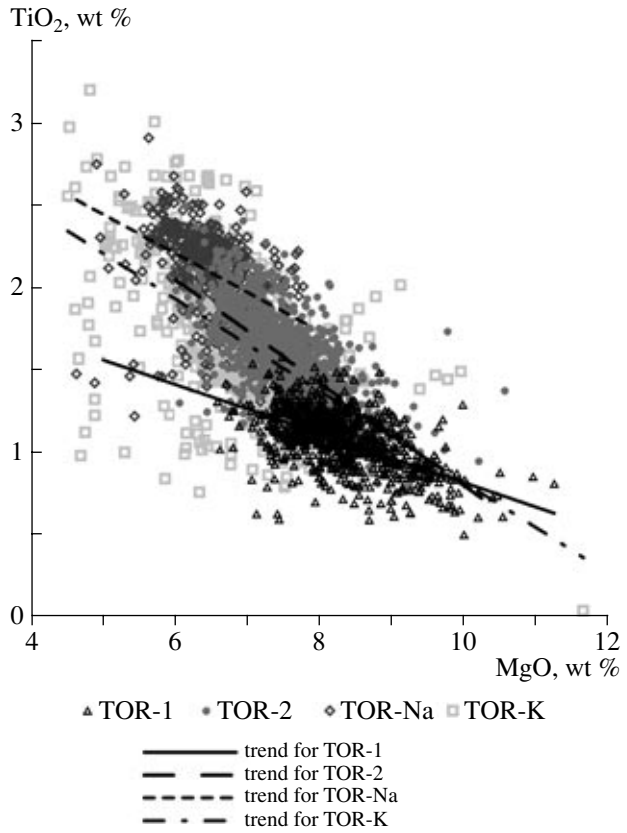

Fig. 5. MgO–TiO_2 diagram for the compositional fields and differentiation trends of TOR-1, TOR-2, TOR-Na, and TOR-K. The different slopes of the differentiation trends and different TiO_2 contents accentuate the role of TiO_2 as an indicator of plume and spreading associations of basalts (see text).

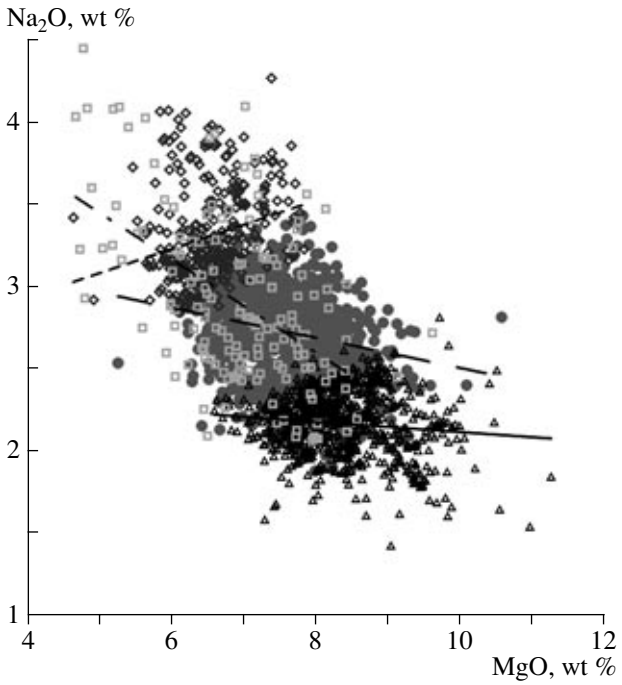

Fig. 6. MgO–Na_2O diagram for the compositional fields and differentiation trends of TOR-1, TOR-2, TOR-Na, and TOR-K. The different slopes of the differentiation trends and different Na_2O contents accentuate the role of Na_2O as an indicator of plume and spreading associations of basalts (see text). See Fig. 5 for symbol explanations.

the strongly elevated concentration of K_2O and the high degree of enrichment in TOR-K. The fractionation trends for this group are little informative because of the broad compositional variations (Fig. 3). In general, the compositional variations of the TOR-K group illustrate its independence as a group. It has been demonstrated in our earlier publications that TOR-K belongs to the plume association, and its petrological parameters are the most contrasting relative to TOR-Na.

TOR-Fe and TOR-FeTi were classed (Dmitriev, 1998) with the deep fractionation products of TOR-1 and TOR-2, respectively, in magmatic chambers under relatively low (<3 kbar) pressures. Cluster analysis allowed us to demonstrate on a quantitative basis that TOR-Fe and TOR-1 are genetically related within the plume association and TOR-FeTi and TOR-2 within the spreading association. This is clearly demonstrated in Figs. 8 and 9: the variations in the TiO_2 and Na_2O contents of TOR-Fe lie on the continuation of the differentiation trend for TOR-1, and the analogous variations for TOR-FeTi continue the trend for TOR-2.

In our pervious studies, we have calculated the pressures, temperatures, and H_2O concentrations for the triple TOR cotectic (*Ol–Pl–Cpx*) by the method described in (Dmitriev et al., 1994) and then implemented as an option of the PETROLOG software package (Danyushevsky et al., 1996). The method for estimating pressure during TOR crystallization is underlain by the effect of the expansion of the clinopyroxene stability field with increasing pressure. To solve this problem, a series of polybaric calculations was conducted to simulate the crystallization temperatures of olivine, plagioclase, and clinopyroxene under various pressures. The condition of the equality of the calculated temperatures for the quenched glasses is a criterion for the evaluation of the pressure within the stability field of this mineral assemblage. The concentration of water is estimated based on the known effect of a decrease in the plagioclase liquidus temperature relative to those of olivine and clinopyroxene. Currently available extensive information on the petrography and petrochemistry of TOR indicates that, at MgO > 9 wt %, crystallization starts with olivine, and the stable *Ol–Pl–Cpx* triple mineral assemblage appears when the MgO content decreases to 8.5 wt % or less. This makes it possible to apply this method regardless of the crystallization conditions (iso- or polybaric).

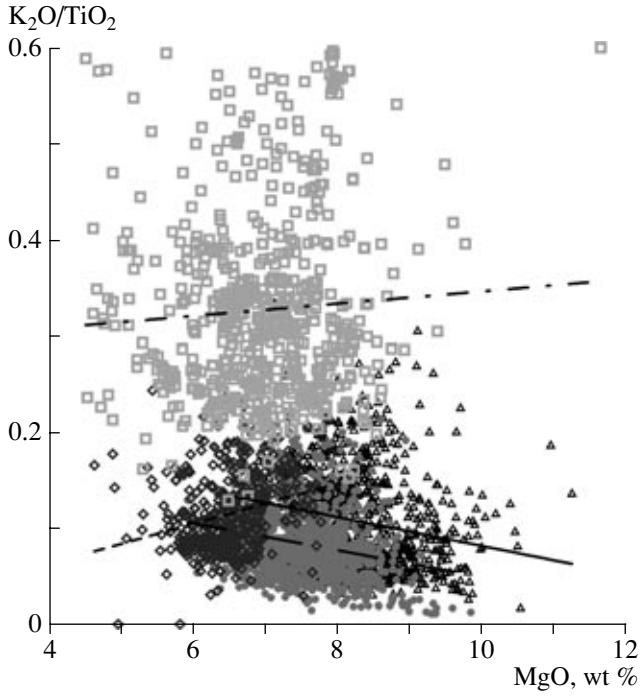

Fig. 7. MgO–K_2O/TiO_2 diagram for the compositional fields and differentiation trends of TOR-1, TOR-2, TOR-Na, and TOR-K. The different slopes of the differentiation trends and different K_2O/TiO_2 ratios demonstrate the different enrichment of various TOR groups and their derivation from distinct mantle sources (see text). See Fig. 5 for symbol explanations.

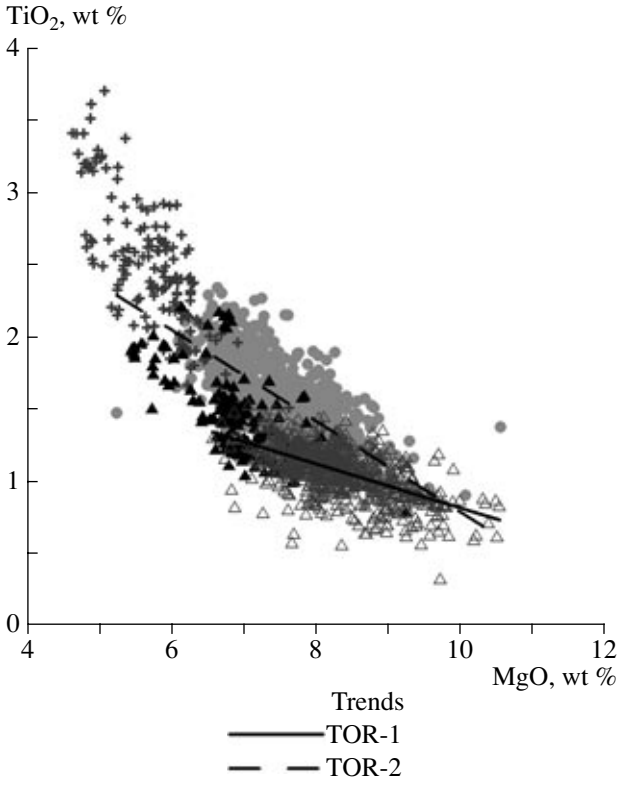

Fig. 8. MgO–TiO_2 diagram for the compositional fields and differentiation trends of TOR-1, TOR-2, TOR-Fe, and TOR-FeTi. The diagram highlights genetic relations of TOR-Fe with TOR-1 and of TOR-FeTi with TOR-2. See Fig. 3 for symbol explanations.

The results of these calculations enabled us to estimate the major tendencies in the distribution of the compositions of various TOR groups in *P–T* space and to evaluate the limits for the water concentrations in the corresponding melts during their differentiation.

Below we present the results of analogous calculations conducted by the modernized PETROLOG 2 software (Danyushevsky, 2001), which allowed us to notably refine the location of the compositional TOR groups in *P–T* space. The pressure is estimated by this program accurate to ±2 kbar, and the accuracy of the temperature values is within the accuracy of the used geothermometers (5–10°C). The water concentrations in the melt can be evaluated accurate to approximately 50% of the calculated contents.

Figure 10 displays a MgO–H_2O diagram for the calculated water concentrations in all TOR groups. Note that these calculated H_2O concentrations in TOR are consistent with the direct determinations of water in MORB of various compositions (Kovalenko et al., 2004; Asimov and Langmuir, 2003; Sobolev, 1997). These data will be used below to calculate differentiation trends for TOR of different groups.

Figure 11 shows the compositional fields of the six TOR groups in *P–T* space. It can be clearly seen that the common field is divided into "strata" parallel to the lines of dry solidi (Herzberg, 1996) corresponding to discrete TOR groups. These strata do not intersect, which directly testifies that the sources of each TOR group are different and they evolve independently, along parallel trends. The overlaps of the fields are insignificant, a feature indicating the stability of the independent evolutionary processes of the melts derived from different sources. It is also clearly seen that the TOR-1 group comprises the differentiation products of melts derived at the highest temperatures and pressures, and the TOR-Na group was, conversely, produced at the lowest temperature and pressure values. In terms of these parameters, the TOR-2 group occupies a transitional position. The TOR-K group is characterized by the maximum dispersion of its *P–T* parameters, and the compositions plotting within the high-pressure region are shifted toward moderate temperatures. The latter feature could result from the elevated water concentrations in the source of these melts. The TOR-Fe group continues the trend for TOR-1 with a slight shift toward lower temperatures and pressures, and TOR-FeTi makes up the ending of the trend for TOR-2, also with a shift toward the lowest *P–T* parameters.

The average differentiation trends for each TOR group that accentuate the character of their evolution in

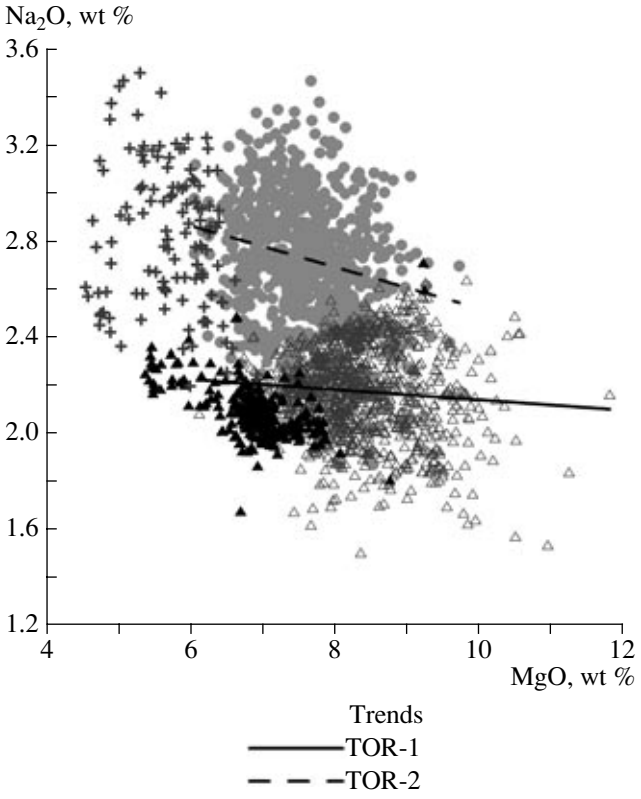

Fig. 9. MgO–Na_2O diagram for the compositional fields and differentiation trends of TOR-1, TOR-2, TOR-Fe, and TOR-FeTi. The diagram highlights genetic relations of TOR-Fe with TOR-1 and of TOR-FeTi with TOR-2. See Fig. 3 for symbol explanations.

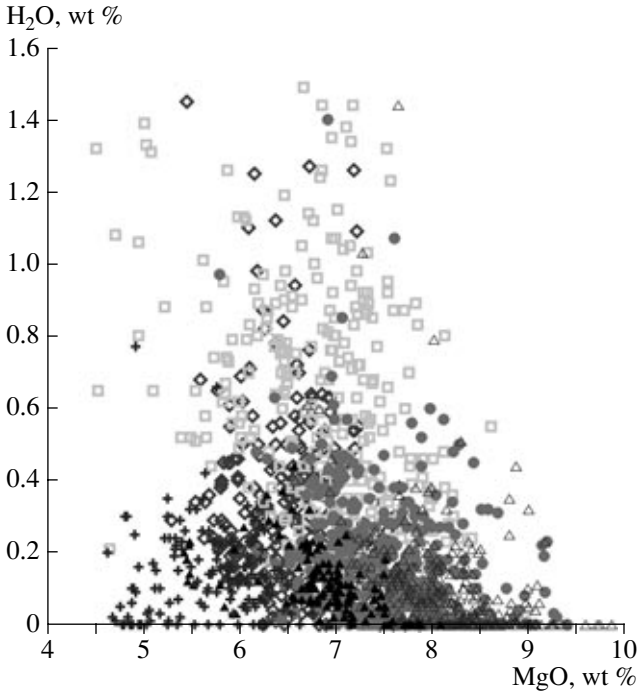

Fig. 10. MgO–H_2O diagram for the compositional fields of major TOR groups. The H_2O concentrations were calculated by the method proposed by Danyushevsky et al. (1996) accurate to ±0.5%. See Fig. 3 for symbol explanations.

a *P–T* diagram, were calculated by the modernized COMAGMAT 3.5 computer program (Ariskin and Barmina, 2004). For these calculations, the average compositions of the most magnesian varieties (initial points of the trends) were calculated for each TOR group from data on the position of their compositional fields in MgO–other major component diagrams. The initial pressure was specified from the *P–T* coordinates of these compositions (Fig. 11). The differentiation conditions were determined by selecting parameters at which the visually estimated position of the calculated trend is in good agreement with the position of the compositional fields in the MgO–other major component diagrams. During this stage of the research, there was no need to calculate the function measuring the deviations of natural compositions from the trend, because this value turned out to be smaller than the overlap intervals of the fields of various TOR groups. The H_2O concentrations in each group were roughly evaluated from Fig. 10 (see above). As a result of this selection, it was established that the variations in TOR compositions are most consistent with the model of fractional crystallization with a *dP*/*dF* step (kbar/mol, %) of 0.1–0.4, in an open system, during decompression at the QFM buffer. The differentiation trend for TOR-K was calculated at an initial pressure of 10 kbar, because the COMAGMAT 3.5 program ceased to be accurate enough at higher pressures. All of the aforementioned parameters and the calculated temperature values from the beginning of crystallization to the cotectic are summarized in Table 2 (these parameters for TOR-K were calculated for a pressure range of 0–10 kbar, see above).

Figure 12 displays the fractional crystallization trends for all TOR groups in a *P–T* diagram. The diagram also shows the compositional data points of the parental melts of TOR-1, TOR-2, and TOR-K, which were determined experimentally (Table 3), and the possible compositional fields of these melts.

REGIONAL DISTRIBUTION OF TOR GROUPS

The coverage of mid-oceanic ridges with TOR analyses is illustrated by Table 4, which demonstrates that the ridges in the North Atlantic and Pacific oceans are sampled practically equally thoroughly and are close in this respect to the crust basement of the ocean as a whole: an average of 1 analysis per 2 km along the ridge strike. This allowed us to fairly reliably compare the variations in the TOR compositions in these areas. Analogous comparison of data on the South Pacific and Indian oceans should be conducted more cautiously.

The overall distribution of various TOR groups over the ocean (Table 1) is illustrated by a histogram for discriminant D-04, which makes it possible to identify the affiliation of various TOR groups with the plume or spreading associations (Fig. 13). D-04 was calculated based on the same key arguments that were used for version 5 of cluster analysis: TiO_2, Na_2O, K_2O, Na_2O/MgO, and K_2O/TiO_2.

The two compared files included TOR-1 + TOR-K (plume association) and TOR-2 + TOR-Na (spreading association). According to the calculations, D-04 = 6.43 TiO_2 + 7.95 Na_2O – 19.41 K_2O –19.91 Na_2O/MgO + 0.95 K_2O/TiO_2. The critical value is $D\text{-}04_0$ = 19.28 (the boundary between the plume and spreading associations). Figure 12 indicates that these associations are divided by a clearly pronounced minimum: the overlap zone for TOR-1 and TOR-2 does not exceed 10% of the whole body of data, and the compositions of TOR-Na and TOR-K plot on the D-04 axis with a gap. The compositions of TOR-Fe and TOR-FeTi were not included in the "teaching" file, but they plot on the D-04 axis in corresponding ranges and are divided by a gap: TOR-Fe occurs within the plume association, and TOR-FeTi plots within the spreading association, a fact corroborating their classification (see above) and justifying the accurateness and efficiency of the D-04 discriminant. Figure 13 reflects the proportions of the plume and spreading associations and various TOR groups for the ocean as a whole (see also text above and Table 1).

Table 5 reports data on the composition and distribution of various TOR groups in major regions of the ocean, which were calculated during our research. The most significant differences in the distribution of plume and spreading basalt associations and various TOR groups can be seen when the northern segment of MAR is compared with EPR, as was previously mentioned in (Dmitriev, 1998; Dmitriev and Sokolov, 2002). In these

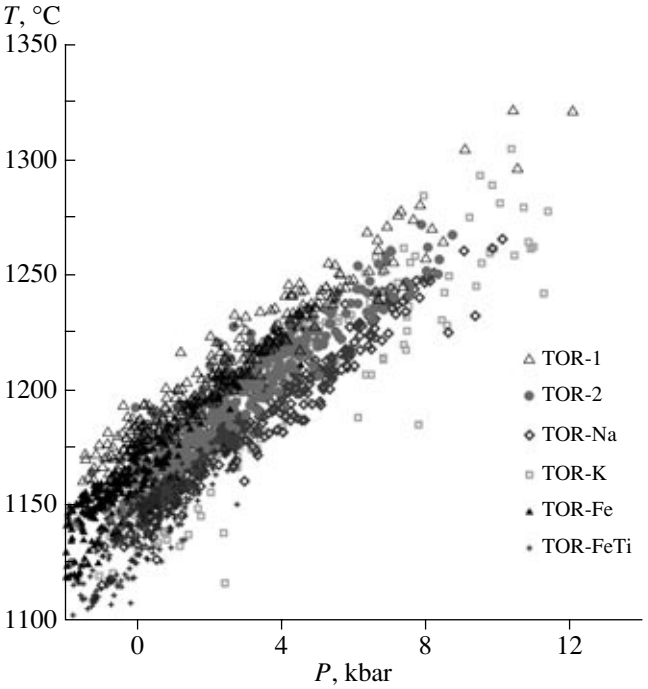

Fig. 11. *P–T* diagram for the composition of six TOR groups. The parameters were calculated by the computer program developed by Danyushevsky et al. (1996) accurate to ±2 kbar and ±10°C.

Table 2. Composition (wt %) of the most magnesian TOR varieties and their parameters used to calculate the differentiation trends

Component	Plume association			Spreading association		
	TOR-1	TOR-K	TOR-Fe	TOR-2	TOR-Na	TOR-FeTi
SiO_2	49.2	49.9	50.9	50.1	51.5	51.0
TiO_2	0.7	1.2	1.2	1.2	1.6	2.0
Al_2O_3	17.7	17.5	15.0	17.2	16.2	13.5
FeO	7.5	8.0	11.5	8.7	9.5	13.0
MgO	11.0	9.0	7.7	8.7	7.5	6.9
CaO	11.8	11.5	11.5	11.4	10.2	10.7
Na_2O	2.0	2.5	2.1	2.6	3.3	2.8
K_2O	0.1	0.4	0.1	0.1	0.2	0.1
P	10	10	2	8	7	2
H_2O	0.1	0.5	0.2	0.2	0.3	0.2
dP/dF	0.2	0.3	0.1	0.2	0.2	0.1
T	1300 *Ol*	1250 *Ol* + *Pl*	1190 *Ol* + *Pl*	1260 *Pl*	1200 *Ol* + *Pl*	1180 *Ol*
T	1280 *Ol* + *Pl*		1150 *Ol* + *Pl* + *Aug*	1240 *Pl* + *Ol*		1160 *Ol* + *Pl* + *Aug*
T_{cotect}	1160 *Ol* + *Pl* + *Aug*	1140 *Ol* + *Pl* + *Aug*	1120 *Pig* + *Pl* + *Aug*	1150 *Pl* + *Ol* + *Aug*	1140 *Ol* + *Pl* + *Aug*	1080 *Ol* + *Pl* + *Aug* + *Mt*

Note: *dP/dF* is the degree of fractionation, kbar/mol; *T*, °C is the temperature variations in the course of crystallization and changes in mineral assemblages. (*Ol*) olivine, (*Pl*) plagioclase, (*Aug*) augite, (*Mt*) magnetite, (*Pig*) pigeonite.

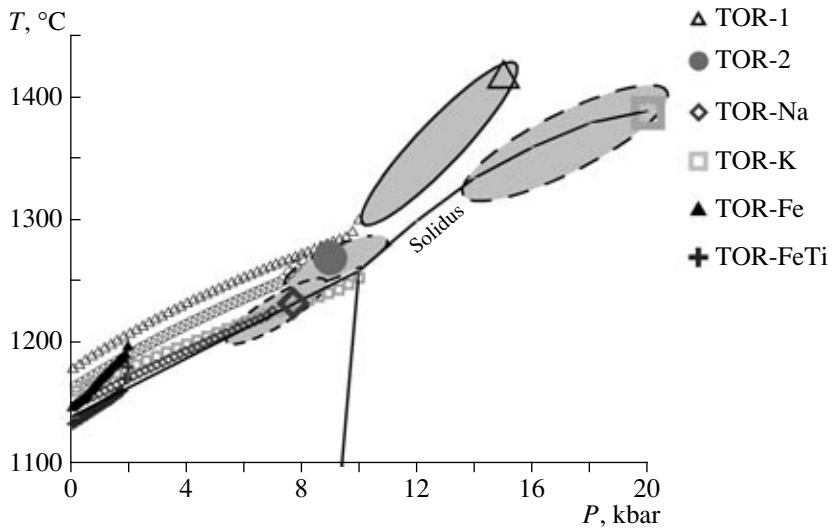

Fig. 12. Fractional crystallization trends for the six groups of basalts from the global system of mid-oceanic ridges (TOR) calculated by the COMAGMAT 3.5 computer program (Ariskin, 1999) and the fields of *P–T* parameters under which the parental melts were derived. The dry solidus line is given after (Herzberg and Zhang, 1996). See text for explanations.

papers, the phenomenon is explained in light of data on the differences between the spreading velocities in MAR and EPR. It was demonstrated that an increase in the spreading velocity (EPR) is coupled with an increase in the percentage of spreading associations relative to plume ones due to the association of mantle upwelling with a high spreading velocity. The geodynamic and petrological consequences of these differences are discussed in detail and the aforementioned publications.

Table 3. Composition (wt %) of parental TOR melts according to data obtained on melt inclusions and numerical simulations

Component	TOR-1 (Sobolev and Dmitriev, 1989)	TOR-2 (Sobolev and Dmitriev, 1989)	TOR-K (Gurenko *et al.*, 1999)
SiO_2	48.9	49.6	46.5
TiO_2	0.5	0.9	2.1
Al_2O_3	15.7	18.6	13.9
FeO	7.7	7.2	8.7
MgO	13.9	9.4	12.6
CaO	11.8	12.0	12.5
Na_2O	1.5	2.3	2.2
K_2O	0.0	0.0	0.8
K_2O/TiO_2			0.38
P, kbar	15	9	20
T, °C	1420	1270	1388

Figure 14 clearly demonstrates the differences between the volumetric proportions of plume and spreading basalt associations and the volumetric proportions of various TOR groups at different spreading velocities, as is illustrated by the example of D-04 histograms for the northern segment of MAR (Fig. 13a) and EPR (Fig. 13b) and as is also demonstrated in Table 4. Figure 14 clearly demonstrates the strong predominance of the spreading association in EPR compared with MAR (88 and 12%), mostly because of an increase in the percentage of TOR-2 relative to TOR-1. The volume of TOR-Na is notably higher in EPR than in the northern segment of MAR, while TOR-K is developed mainly in MAR. TOR-FeTi (spreading association) is fairly abundant in EPR and practically absent from MAR. TOR-Fe (plume association) are widespread in MAR, where they are spatially restricted to the Reykjanes and Kolbeinsey ridges (related to the Iceland megaplume), and occur near the Azores megaplume and in the vicinity of the Bouvet Island plume. TOR-Fe were also found in the Red Sea and Indian Ocean (slow-spreading ridges) but are relatively scarce at EPR. The latter fact is displayed in the map of the distribution of TOR-Fe and TOR-FeTi (Fig. 15).

It was mentioned above that, at slow spreading velocities, there are stable correlations between petrological and geophysical parameters, and the distribution of various TOR groups along the ridge axis is in agreement with its tectono-magmatic segmentation. At high spreading velocities, the correlation between the geophysical and petrological parameters becomes unstable, and this results in a chaotic distribution of various TOR groups and their close spatial association with one another. It has been demonstrated that these differences stem from the fact that an increase in spreading velocity is related to an increase in the inten-

Table 4. Sampling density over the system of mid-oceanic ridges (estimates)

Area	Length, km	Number of analyses	Number of analyses per km
Pacific Ocean, Juan de Fuca Ridge, EPR segment between 56° S and 26° N	11500	6273	0.5
Galapagos spreading center	2350	1249	0.5
North Atlantic, MAR segment between 0°S and 80°S	10200	6053	0.6
Southern Atlantic, MAR segment between 0°S and 60°S and the American-Antarctic Ridge	8100	1735	0.2
Indian Ocean: Red Sea, Mid-Indian Ridge, Southwest Indian Ridge, and Southeast Indian Ridge	13100	552	0.04
Ocean as a whole	45250	18079	0.4

sity of mantle upwelling and an intensification of the productivity of magmatism. This can lead to the obliteration of boundaries between discrete magmatic provinces and the mixing of melts of different genesis.

This can be illustrated by the comparison of the distributions of TOR-Na and TOR-K, i.e., two TOR groups with the most contrasting petrological parameters, at low and high spreading velocities in the northern part of MAR (Fig. 16a) and EPR (Fig. 16b). In these diagrams, the geochemical differences between TOR-Na and TOR-K are highlighted by their different degrees of enrichment (K_2O/TiO_2), and the geophysical fields, whose character is controlled by the geodynamic environments in which the ridges developed, are characterized by the data of satellite altimetry (Sandwell and Smith, 1997) on the surface topography. Figure 16 demonstrates that, at a low spreading velocity (MAR), both TOR groups are notably separated along the ridge trend, with TOR-K and TOR-Na spatially restricted to positive and negative gravity anomalies (topographic features), respectively. At a high spreading velocity (EPR), this distribution pattern is disturbed: both groups occur together within a small area north of the equator but are mostly separated south of it. There are no clear correlations between the distributions of TOR-Na and TOR-K and the gravity field.

DISCUSSION

First of all, it should be mentioned that the principal conclusions concerning the petrological and geodynamic characteristics of oceanic magmatism drawn earlier based on limited material were confirmed by the results of this research and were significantly refined

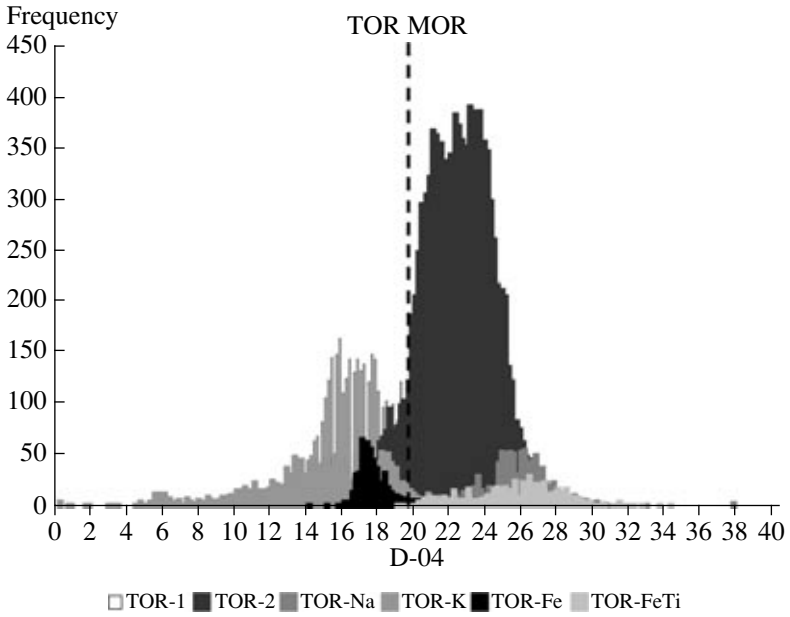

Fig. 13. Histogram of the D-04 discriminant characterizing the volumetric proportions of six TOR rock groups in the global system of mid-oceanic ridges (MOR).

Table 5. Average compositions (X) and deviations (σ) for the six TOR groups from various oceanic areas

Components	TOR-1		TOR-2		TOR-Na		TOR-K		TOR-Fe		TORgo-FeTi	
	X	σ	X	σ	X	σ	X	σ	X	σ	X	σ
East Pacific Rise (N = 6273, Q = 34.70%)												
SiO_2	50.19	0.77	50.65	0.58	50.92	0.62	50.73	0.97	49.80	2.34	50.98	0.76
TiO_2	1.14	0.13	1.63	0.31	2.22	0.19	1.84	0.41	1.30	0.68	2.56	0.30
Al_2O_3	15.88	0.87	15.01	0.87	14.28	0.73	15.79	1.24	15.09	1.98	13.30	0.62
FeO	9.19	0.67	10.33	1.05	11.80	1.01	9.69	1.23	12.21	0.88	13.79	0.66
MgO	8.55	0.51	7.55	0.68	6.38	0.51	6.95	0.79	7.70	1.34	5.77	0.42
CaO	12.52	0.42	11.81	0.51	10.79	0.64	11.04	0.99	11.49	0.78	10.17	0.54
Na_2O	2.33	0.14	2.75	0.21	3.17	0.19	3.09	0.39	2.26	0.44	3.01	0.24
K_2O	0.08	0.04	0.13	0.06	0.23	0.06	0.60	0.26	0.07	0.05	0.19	0.06
K/Ti	0.07	0.03	0.08	0.04	0.11	0.03	0.33	0.12	0.05	0.01	0.07	0.02
n	404		4700		486		338		8		337	
q	6.4		74.9		8		5		0		5	
Mid-Atlantic Ridge (N = 7788, Q = 43.08%)												
SiO_2	51.01	0.79	50.92	0.72	51.22	0.55	51.33	1.02	51.09	0.43	50.71	0.84
TiO_2	1.08	0.18	1.52	0.24	2.06	0.24	1.65	0.47	1.35	0.17	1.94	0.40
Al_2O_3	15.40	0.73	15.49	0.69	15.14	0.61	15.71	0.93	14.14	0.28	13.41	0.49
FeO	9.57	0.79	9.94	0.81	10.65	0.86	9.40	1.27	12.34	0.40	14.28	0.94
MgO	8.20	0.72	7.65	0.58	6.60	0.38	7.09	0.99	7.04	0.32	6.04	0.50
CaO	12.34	0.55	11.46	0.51	10.62	0.48	11.26	1.07	11.78	0.37	10.94	0.59
Na_2O	2.16	0.18	2.78	0.26	3.37	0.24	2.81	0.51	2.06	0.10	2.33	0.28
K_2O	0.14	0.06	0.13	0.06	0.22	0.07	0.55	0.22	0.11	0.04	0.19	0.07
K/Ti	0.13	0.05	0.09	0.04	0.11	0.04	0.34	0.11	0.08	0.03	0.09	0.02
n	2342		3583		277		1074		399		113	
q	30.07		46.01		3.56		13.79		5.12		1.45	
Indian Ocean (N = 552, Q = 3.05%)												
SiO_2	51.24	1.14	51.30	0.85	51.27	0.41	51.52	0.79	51.24	1.43		
TiO_2	0.99	0.21	1.39	0.21	1.72	0.18	1.58	0.28	1.29	0.18		
Al_2O_3	15.36	0.97	15.57	0.92	16.41	0.72	15.56	0.88	14.45	0.63		
FeO	9.58	1.12	9.56	1.00	8.84	0.77	9.76	1.34	12.12	0.17		
MgO	8.18	0.80	7.66	0.55	7.20	0.45	6.93	0.73	7.10	0.47		
CaO	12.35	0.59	11.36	0.64	10.42	0.67	11.07	0.80	11.35	0.23		
Na_2O	2.14	0.27	2.85	0.35	3.77	0.25	2.98	0.39	2.22	0.04		
K_2O	0.09	0.04	0.14	0.06	0.23	0.06	0.43	0.13	0.12	0.05		
K/Ti	0.09	0.03	0.10	0.05	0.13	0.02	0.28	0.09	0.09	0.03		
n	96		397		26		29		4			
q	17.40		71.92		4.71		5.25		0.72			
Galapagos spreading center (N = 1249, Q = 6.91%)												
SiO_2	50.33	0.65	50.91	0.67	51.87	0.44	49.52	0.72	51.61	0.33	51.04	0.73
TiO_2	1.04	0.14	1.52	0.31	2.08	0.21	2.00	0.38	1.45	0.10	2.45	0.56
Al_2O_3	15.81	0.65	14.75	0.97	15.60	0.46	17.15	0.88	13.85	0.53	12.92	0.68
FeO	9.43	0.50	10.98	1.51	9.72	0.67	9.14	0.57	11.90	0.35	14.80	1.55
MgO	8.61	0.58	7.45	0.71	6.51	0.57	6.91	0.62	7.39	0.24	5.62	0.66
CaO	12.49	0.34	11.71	0.73	9.90	0.56	10.91	0.74	11.51	0.11	10.29	0.59
Na_2O	2.13	0.16	2.44	0.26	3.77	0.23	3.33	0.34	2.16	0.04	2.53	0.18
K_2O	0.07	0.03	0.11	0.07	0.28	0.05	0.72	0.23	0.05	0.06	0.15	0.05
K/Ti	0.07	0.02	0.07	0.04	0.14	0.02	0.36	0.09	0.03	0.04	0.06	0.02
n	494		356		109		68		8		214	
q	39.56		28.50		8.73		5.44		0.64		17.13	

Table 5. (Contd.)

Components	TOR-1		TOR-2		TOR-Na		TOR-K		TOR-Fe		TOR-FeTi	
	X	σ	*X*	σ	*X*	σ	*X*	σ	*X*	σ	*X*	σ
Mid-Atlantic Ridge (northern segment, $N = 6053$, $Q = 33.48\%$)												
SiO_2	51.03	0.77	50.97	0.75	51.47	0.77	51.44	1.01	51.09	0.42	50.68	0.86
TiO_2	1.08	0.18	1.50	0.24	1.97	0.22	1.54	0.38	1.35	0.16	1.92	0.41
Al_2O_3	15.37	0.70	15.45	0.70	15.06	0.54	15.76	0.83	14.13	0.27	13.35	0.45
FeO	9.60	0.78	9.98	0.84	10.66	0.75	9.14	1.13	12.33	0.40	14.35	0.93
MgO	8.19	0.72	7.64	0.60	6.51	0.41	7.25	0.91	7.04	0.32	6.06	0.49
CaO	12.34	0.55	11.47	0.51	10.55	0.62	11.41	1.05	11.79	0.33	11.03	0.51
Na_2O	2.16	0.18	2.74	0.27	3.41	0.34	2.71	0.48	2.06	0.07	2.26	0.12
K_2O	0.14	0.06	0.13	0.06	0.19	0.09	0.55	0.23	0.11	0.04	0.18	0.06
K/Ti	0.13	0.05	0.09	0.04	0.10	0.06	0.35	0.11	0.08	0.03	0.09	0.02
n	2232		2422		57		840		397		105	
q	36.87		40.02		0.94		13.88		6.56		1.73	
Mid-Atlantic Ridge (southern segment, $N = 1735$, $Q = 9.60\%$)												
SiO_2	50.62	1.00	50.80	0.62	51.16	0.45	50.94	0.97	52.07	0.12	51.08	0.12
TiO_2	1.09	0.21	1.55	0.22	2.08	0.24	2.06	0.53	1.99	0.04	2.27	0.07
Al_2O_3	16.06	0.97	15.57	0.67	15.16	0.62	15.55	1.20	14.90	0.10	14.20	0.03
FeO	9.05	0.77	9.87	0.75	10.65	0.89	10.32	1.29	13.36	0.19	13.32	0.09
MgO	8.49	0.67	7.68	0.55	6.62	0.37	6.50	1.05	6.66	0.03	5.77	0.20
CaO	12.23	0.53	11.44	0.49	10.64	0.44	10.73	0.98	9.69	0.58	9.76	0.12
Na_2O	2.28	0.23	2.85	0.24	3.36	0.21	3.14	0.45	1.18	0.35	3.24	0.04
K_2O	0.08	0.06	0.13	0.07	0.22	0.06	0.57	0.19	0.15	0.05	0.29	0.04
K/Ti	0.07	0.06	0.08	0.04	0.11	0.04	0.28	0.08	0.07	0.03	0.13	0.02
n	110		1161		220		234		2		8	
q	6.34		66.92		12.68		13.49		0.11		0.46	

Note: *N* is the number of analyses for a given area, *Q* its percentage of the overall number of the analyses used, *n* is the number of analyses for each TOR group and the percentage of their sampling *q* in a given area.

with the application of formal statistical analysis (cluster analysis, analysis of histograms and covariations of key parameters, and discriminant analysis) to the whole volume of data on the compositions of the quenched basaltic glasses from the seafloor.

The six major stable TOR groups remained the same, but the variation ranges of their compositions were significantly refined, and their affiliation with plume or spreading associations was determined more accurately.

The application of the modernized computer program PETROLOG 2 (Danyushevsky, 2001) and a new version of the COMAGMAT 3.5 program (Ariskin and Barmina, 2004) to the refined data on the compositional variations of discrete TOR groups allowed us to evaluate more accurately their differentiation in pressure–temperature diagrams and to localize the differentiation trends on a quantitative basis. The comparison of these trends with data on the *P–T* parameters under which the parental melts were derived from the mantle (these parameters were established experimentally) has demonstrated that the major TOR groups are indeed produced by different parental mantle melts, and the mixing of their differentiation products during their ascent to the surface either is limited or does not take place at all.

Of course, the recognition of the six major groups of basalts was only the first necessary generalization of their complex compositional variations. In practice, each group is fairly heterogeneous, a fact that became more apparent when the whole data body was examined. The reasons for this are numerous and include local compositional characteristics of the mantle

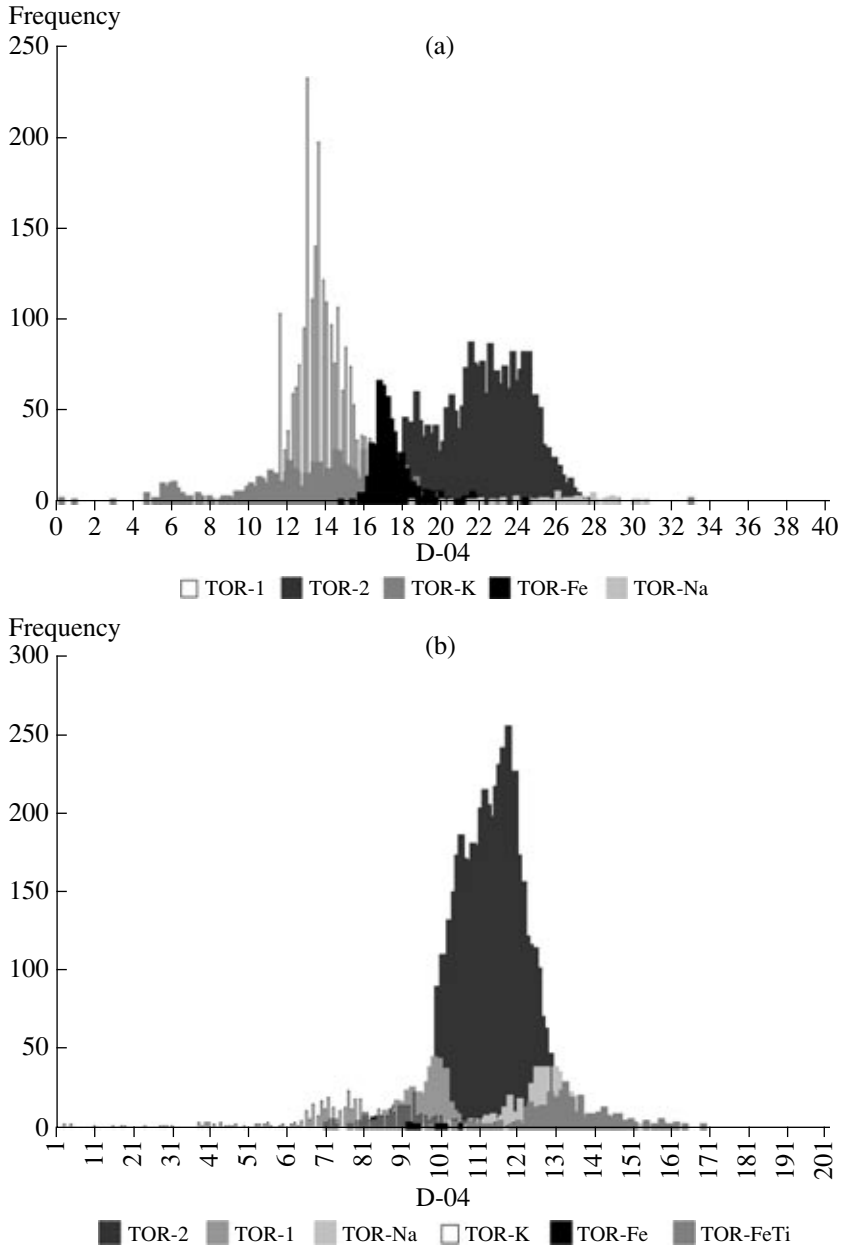

Fig. 14. Changes in the volumetric proportions of various TOR groups depending on the spreading velocity as is illustrated by the D-04 histogram for (a) MAR and (b) EPR. See text for explanations.

source, the geodynamic environments in which the differentiation took place, etc. It is quite probable that further research will lead to a next step of generalization and the recognition of other TOR groups (or subgroups).

It is pertinent to mention some features of the compositional heterogeneity of discrete TOR groups.

TOR-1. The position of the data point of the parental melt of TOR-1, determined experimentally, relative to the corresponding compositional field and trend (Fig. 12) indicates that the TOR-1 sample used to calculate (from the results obtained on melt inclusions; Sobolev and Dmitriev, 1989; Sobolev, 1997) the *P–T* parameters under which the melt was derived from the mantle source is a rare, the most magnesian member of this basalt group. Judging from the orientation of the TOR-1 compositional field in a *P–T* diagram relative to the data point of the TOR-1 parental melt, most of the parental melts of this group can define a fairly broad stripe parallel to the solidus line, and their differentiation can give rise to a complex compositional series.

TOR-2. The compositional variations of this group are the most stable, and the composition of the parental melt determined experimentally lies on the continua-

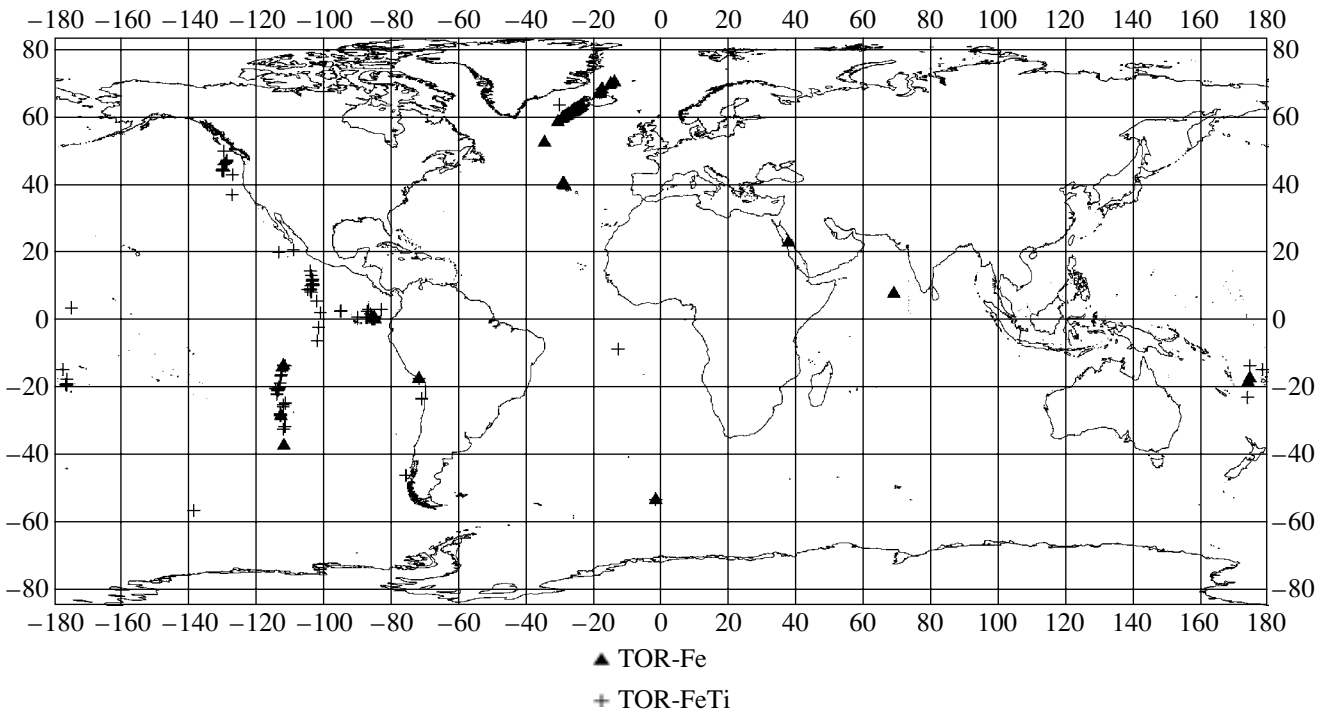

Fig. 15. Schematic map for the distribution of TOR-Fe and TOR-FeTi in the World Ocean. TOR-Fe and TOR-FeTi obviously dominate in the northern MAR segment and at EPR, respectively.

tion of the TOR-2 field in a *P–T* diagram. The basalts of this group are spread most widely in the global system of mid-oceanic ridges, and the relative stability of their compositions can be caused by the optimum geodynamic conditions of the magmatism of the whole system.

TOR-Na. The TOR-Na group is of exclusive interest because its evolution takes place at the lowest pressures and temperatures and within the overall minimum range of depths. This was previously explained by the unusual geodynamic environment of mantle magmatism in slow-spreading ridges, which is characterized by the lowest productivity of volcanism at the cold, rigid lithosphere and the development of the Hess crust (Dmitriev, 1998; Dmitriev et al., 1999; Dmitriev and Sokolov, 2002, 2003; Bonatti et al., 2001, 2003; Klein and Langmuir, 1987; Langmuir et al., 1992). Our present research has proved that TOR-Na are also spread fairly widely at the East Pacific Rise, a ridge with the maximum spreading velocity. This fact calls for its further examination with the use of reliable information on the deep structure of EPR and the heterogeneity of its upper levels. Conceivably, such a research will make it possible to solve the problems concerning the preservation of cold lithosphere blocks during the intense upwelling of heated mantle (a process that brings about fast spreading), the sizes of these blocks, their compositional heterogeneity, and their interaction with the mantle. The solution of these problems will be undoubtedly facilitated by the detailed studying of the compositional variations of the TOR-Na themselves, which can, perhaps, comprise two subgroups that differentiate at two pressure levels (>3 kbar and <3 kbar), as can be seen in Fig. 17. This highlights the need for experimental determining the composition of the parental melt (or melts) of TOR-Na and the conditions under which it (or they) are derived from the mantle. This research seems to be crucial from the viewpoint of the petrology, geochemistry, and geodynamics of oceanic mantle magmatism.

TOR-K. This group of basalts displays the maximum dispersion of their compositions and the broadest range of the *P–T* parameters of fractionation, which overlaps the compositional fields of all other basalt groups and even extends outside of them. This feature of the TOR-K group can be explained as follows. According to its petrological and geochemical characteristics, this group is transitional to a large individual and complicated group of basalts whose sources occur in the lower mantle or in its transitional zone to the upper mantle. In various classifications, these basalts are attributed to within-plate or island (OIB) rocks or to the products of magmatism related to plumes, hotspots, mantle jets, etc. Despite terminological differences, the common mechanism thought to initiate this type of magmatism is mantle melting in response to its active local upwelling from significant depths, with breaking through the surrounding lithospheric structures and the origin of overprinted chambers of geochemically enriched basalts of broad compositional range. Accord-

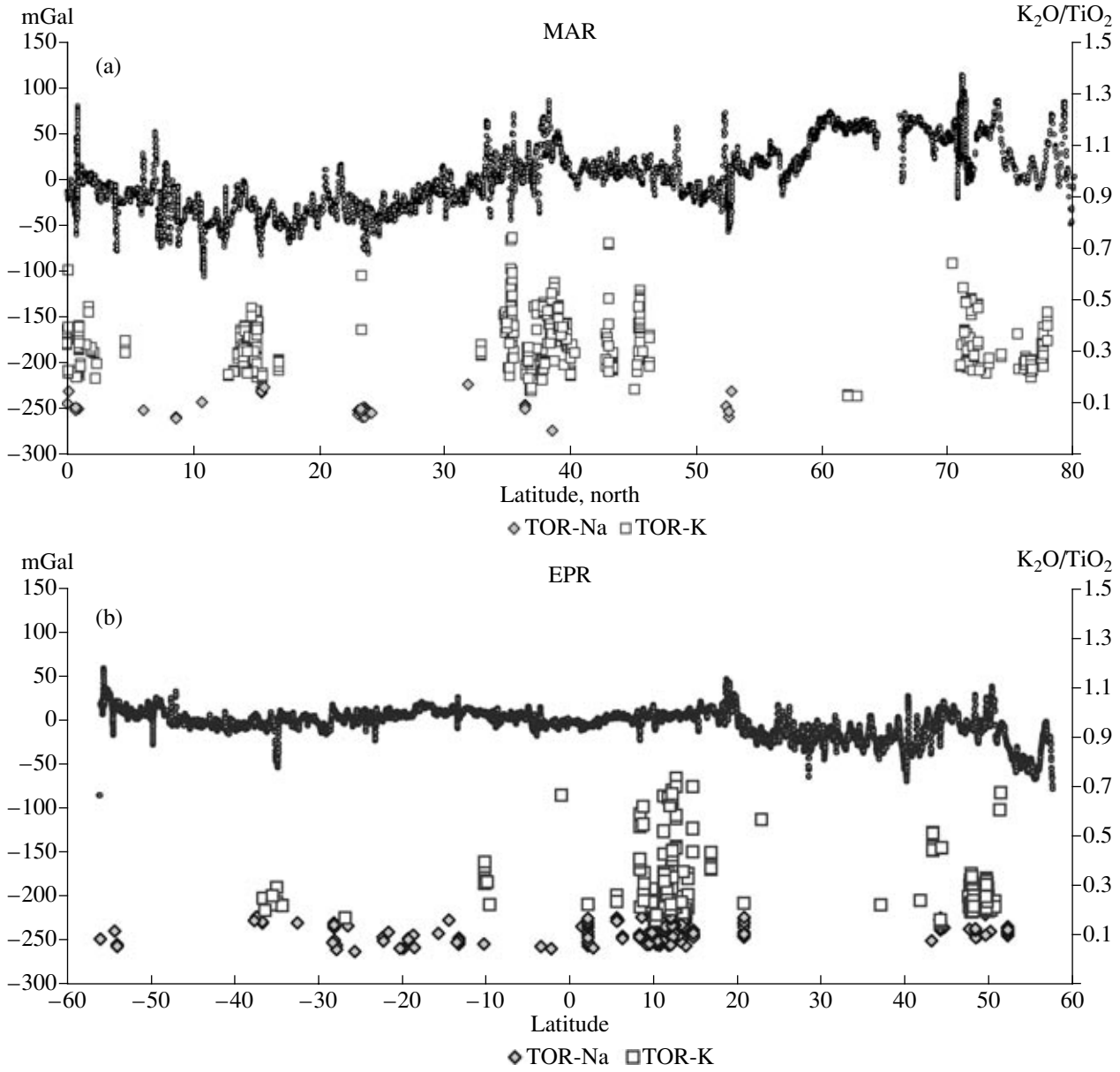

Fig. 16. Comparison of the distributions of TOR-Na and TOR-K and their correlations with free-air gravity anomalies (Sandwell and Smith, 1997) along the axis of (a) the northern part of MAR and (b) EPR. See text for explanations.

ing to these features, we ascribed the TOR-K group to the plume association of basalts of mid-oceanic ridges. The broad compositional variations of this group can also be caused by the broad range of parameters under which the parental melts are derived from compositionally various mantle sources. Because of this, the detailed examination of the compositional heterogeneity of the basalts of the TOR-K group and the elucidation of the reasons for these heterogeneities is one of the crucial problems of the petrology, geochemistry, and geodynamics of mantle magmatism in mid-oceanic ridges.

TOR-Fe and TOR-FeTi. Each of these groups is quite homogeneous in composition, which can be explained by narrow ranges of the fractionation parameters of these rocks in intermediate magma chambers at low pressures. The homogeneity of each group is also retained in terms of the concentration levels of indicator elements (Ti, Na, and K), a feature indicating that these TOR groups are derivatives of either TOR-1 (TOR-Fe) or TOR-2 (TOR-FeTi). This can result from the absence of mixing between plume and spreading associations at the depth levels where the magma chambers are formed. Further research should be centered on the identification of ferrous and ferrous–titanic basalts as derivatives of TOR-Na and TOR-K.

An important outcome of our research is the refining of the distribution of various TOR groups in the system

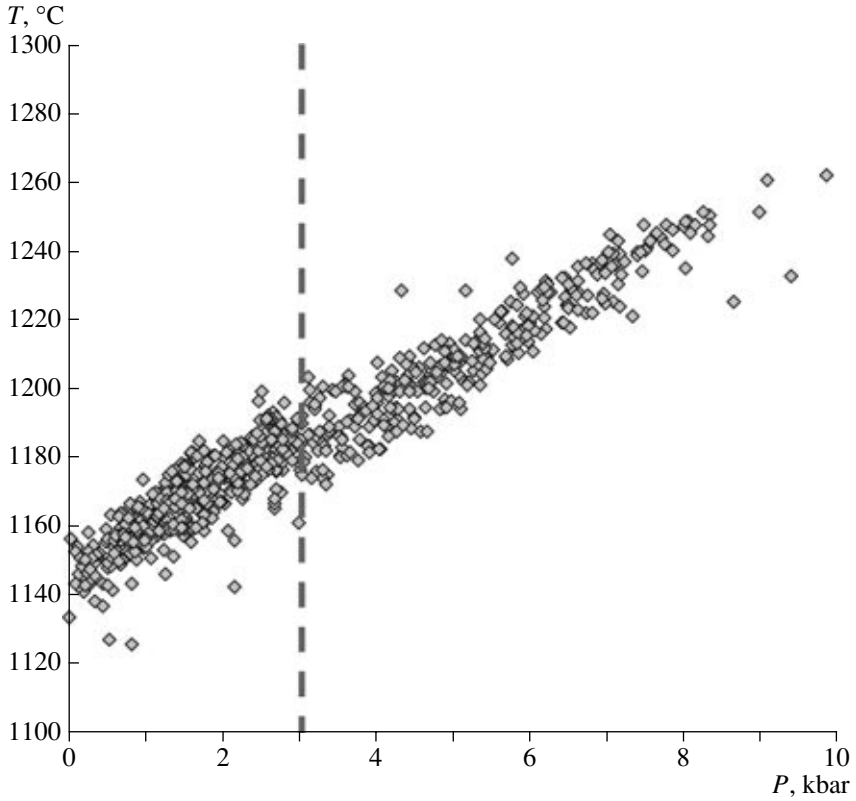

Fig. 17. *P–T* diagram for the compositional field of TOR-Na. The dashed line corresponds to the boundary between two possible subgroups of TOR-Na.

of mid-oceanic ridges. The most interesting data were obtained on an increase in the volumes of spreading basaltic associations, including the group of TOR-Na, in the EPR system and a significant increase in the volume of the TOR-K group in the plume basalt association of MAR. This confirms in quantitative terms the earlier conclusion that the distribution of various TOR groups (which are the evolutionary products of sources at different depths in the mantle) depends on the dynamics of its upwelling and the velocity of spreading.

CONCLUSIONS

The formal statistical analysis of the compositional variations of basalts for the whole global system of mid-oceanic ridges yielded important results. New data were obtained on the petrological parameters of the evolution of mantle magmatism and the spatial distribution of characteristics of its products depending on the geodynamic environments. These results made it possible to assay the current availability of petrological information on magmatism in mid-oceanic ridges and to propose the following scheme for identifying various TOR groups among newly obtained data on quenched glasses:

(1) the affiliation to plume or spreading associations based on the discriminant value of D-04 = 6.43 TiO_2 + 7.95 Na_2O – 19.41 K_2O – 19.91 Na_2O/MgO + 0.95 K_2O/TiO_2. Compositions with D-04_0 < 19.28 are attributed to the plume association and those with D-04_0 > 19.28 are related to the spreading association;

(2) compositions of the plume association with FeO > 11 wt % are ascribed to TOR-Fe, and compositions of the spreading association with FeO > 13 wt % are classed with TOR-FeTi;

(3) the TOR-K group comprises compositions of the plume association with K_2O > 0.4 wt % and FeO < 11 wt %;

(4) the TOR-Na group includes compositions of the spreading association with Na_2O > 3 wt % and FeO < 13 wt %;

(5) the TOR-1 group consists of compositions of the plume association with K_2O < 0.4 wt % and FeO < 11 wt %;

(6) the TOR-2 group comprises compositions of the spreading association with Na_2O < 3 wt % and FeO < 13 wt %.

In order to identify TOR groups, one can use the diagrams presented in Fig. 3 (Na_2O/MgO–K_2O/TiO_2) and Fig. 11 (*P–T*). In the latter, the values for *P* and *T* should be calculated by the PETROLOG 2 computer program (Danyushevsky, 2001).

The groups can always be identified accurate to at least 10%.

The results of our research also make it possible to propose the avenues for further studies.

1. In the course of this research, information was obtained that is needed for the development of the petrological basis for a geodynamic model of magmatism of the six major basalt groups (*P–T* parameters of their evolution, productivity of volcanism, mantle upwelling, spreading, etc.). Since no data on the geochemistry of trace incompatible elements and isotopes were used, detailed information was lost on the geochemical heterogeneity of the mantle sources of magmatism and its influence on the distribution of various TOR groups and on the character of genetic relations between these groups and their associations. Because of this, one of the key goals for the further investigations is the systematizing of factual material on the geochemistry of basalts in mid-oceanic ridges with its correlating with geologic structures and with regard for the affiliation of the rocks with discrete TOR groups.

2. A comparative petrological–geochemical study of the basalts and the rocks of the plutonic complex should be carried out. For example, it is interesting to compare TOR-Fe and TOR-TiFe with dike and intrusive gabbroids.

3. An important independent problem is the examination of relations between the compositions of various TOR groups and the composition of their mantle source. It is particularly interesting to explore the geochemical and geodynamic aspects of this problem.

4. It is necessary to further examine correlations between the petrological–geochemical and geophysical parameters. The statistical justification of the recognition of the six discrete basalt groups made it possible to formulate specific tasks for the studying relations between the evolution of magmatism and the geodynamic environments in which the lithosphere is produced in the mid-oceanic ridges of selected reference areas.

5. Considering the uneven character of sampling in mid-oceanic ridges, it is necessary to systematically collect materials in the South Atlantic and Indian oceans and in polar basins.

ACKNOWLEDGMENTS

The authors thank A.A. Ariskin, Yu.A. Kostitsyn, S.A. Silantyev (Vernadsky Institute of Geochemistry and Analytical Chemistry, Russian Academy of Sciences), and L.V. Danyushevsky (University of Tasmania, Hobart, Tasmania) for fruitful discussion of the manuscript and the outlooks of the further research. This study was supported by the Russian Foundation for Basic Research (project no. 04-05-64905) and the Federal Agency for Science and Innovations, Research School no. NSH-1831.2003.5.

REFERENCES

1. A. A. Ariskin, "Phase Equilibria Modeling in Igneous Petrology: Use of COMAGMAT Model for Simulating Fractionation of Ferro-basaltic Magmas and the Genesis of High-alumina Basalt," J. Volcanol. Geotherm. Res. **90**, 115–162 (1999).
2. A. A. Ariskin and G. S. Barmina "COMAGMAT: Development of a Magma Crystallization Model and its Petrological Applications" Geochem. Int. **42** (Suppl. 1), S1–S157 (2004).
3. P. D. Asimov and C. H. Langmuir, "The Importance of Water to Oceanic Mantle Melting Regimes," Nature **421**, 815–820 (2003).
4. E. Bonatti, M. Ligi, D. Brunelli, et al., "Mantle Thermal Pulses below the Mid-Atlantic Ridge and Temporal Variations in the Formation of Oceanic Lithosphere," Nature **423**, 499–505 (2003).
5. E. Bonatti, M. Ligi, D. Brunelli, et al., "Steady-State Creation of Crust-Free Lithosphere at Cold Spots in Mid Ocean Ridges," Geology **29**, 979–982 (2001).
6. L. V. Danyushevsky, "The Effect of Small Amount of H_2O on Crystallization of Mid-Ocean Ridge and Back-Arc Basin Magmas," J. Volcanol. Geotherm. Res. **110**, 265–280 (2001).
7. L. V. Danyushevsky, A. V. Sobolev, and L. V. Dmitriev, "Estimation of the Pressure of Crystallization and H_2O Content of MORB and BABB Glasses: Calibration of an Empirical Technique," Mineral. Petrol. **57**, 185–204 (1996).
8. L. V. Dmitriev and S. Yu. Sokolov, "Geodynamics of Three Contrasting Types of Oceanic Magmatism and Their Reflection in the Data of Seismic Tomography," Petrologiya **11** (6), 655–672 (2003) [Petrology **11** (6), 597–613 (2003)].
9. L. V. Dmitriev and S. Yu. Sokolov, "Plume and Spreading Basaltic Associations in the Global Mid-Oceanic Ridge System," *Proceedings of International Symposium on Mantle Plumes and Metallogeny, Petrozavodsk, Russia, 2002* (Petrozavodsk, 2002), p. 90 [in Russian].
10. L. V. Dmitriev, "Chemical Variability of Mid-Oceanic Ridge Basalts as a Function of the Geodynamic Setting of Their Formation," Petrologiya **6** (4), 340–362 (1998) [Petrology **6** (4), 314–334 (1998)].
11. L. V. Dmitriev, A. V. Sobolev, L. V. Danyushevsky, et al., "Segmentation of Mid-Atlantic Ridge and Its Relation to the Crystallization Pressure and Water Content in Basaltic Melts," in *Nonlinear Geodynamics*, Ed. by Yu. M. Pushcharovskii (Nauka, Moscow, 1994) [in Russian].
12. L. V. Dmitriev, A. V. Sobolev, M. G. Reisner, et al., "Petrochemical Groups of Quenched Glasses of TOR (Tholeiites of Oceanic Rifts) and their Distribution in the Atlantic and Pacific Oceans," in *Magmatism and Tectonics of the Ocean*, Ed. by Yu. M. Pushcharovskii (Nauka, Moscow, 1990) [in Russian].
13. L. V. Dmitriev, A. V. Sobolev, and N. M. Sushchevskaya, "Primary Melt of Oceanic Tholeiites and the Composition of the Oceanic Upper Mantle," Dokl. Akad. Nauk SSSR **240** (1), 177–180 (1978).
14. L. V. Dmitriev, S. Yu. Sokolov, V. G. Melson, et al., "Plume and Spreading Associations of Basalts in the Mid-Atlantic Ridge and Their Reflection in Petrological

and Geophysical Characteristics," Ross. Zh. Nauk o Zemle **1** (6), 457–476 (1999).

15. A. A. Gurenko, A. V. Sobolev, and N. N. Kononkova, "New Petrological Data on Icelandic Rift Alkali Basalts," Geokhimiya, No. 9, 1262–1274 (1991).
16. C. Herzberg and J. Zhang, "Melting Experiments on Anhydrous Peridotite KLB-1: Composition of Magmas in the Upper Mantle and Transitional Zone," J. Geophys. Res. **101** (4), 8271–8295 (1996).
17. E. Jarosevich, J. A. Nelen, and J. A. Norberg, "Electron Microprobe Reference Samples for Mineral Analyses," Smith. Contrib. Earth Sci. **22**, 68–72 (1979).
18. E. M. Klein and C. H. Langmuir, "Global Correlation of Ocean Ridge Basalt Chemistry with Axial Depth and Crustal Thickness," J. Geophys. Res. **92**, 8089–8115 (1987).
19. V. I. Kovalenko, A. V. Girnis, V. A. Dorofeeva, et al., "Magma Sources of Ocean Islands," Dokl. Akad. Nauk **398** (3), 379–384 (2004) [Trans. Russ. Acad. Sci., Earth Sci. Sec. **398** (7), 995 (2004)].
20. C. H. Langmuir, E. M. Klein, and T. Plank, "Petrological Systematics of Mid-Ocean Ridge Basalts: Constraints on Melt Generation Beneath Ocean Ridges," in *Mantle Flow and Melt Generation at Mid-Ocean Ridges*, Ed. by J. Phipps-Morgan, D. K. Blackman, and J. M. Sinton (Am. Geophys. Union, Washington, DC, 1992), pp. 183–280.
21. G. A. McDonald and T. Katsura, "Chemical Composition of Hawaiian Lavas," J. Petrol. **5**, 82–133 (1962).
22. W. G. Melson, G. R. Byerly, et al., "A Catalog of Major Element Chemistry of Abyssal Volcanic Glasses," Smith. Contrib. Earth Sci. **19**, 31–60 (1977).
23. Ridge Petrological Data Base. LDEO. 1999 (http://petdb.ldeo.columbia.edu/petdb/).
24. D. T. Sandwell and W. H. F. Smith, "Marine Gravity Anomaly from Geosat and ERS-1 Satellite Altimetry," J. Geophys. Res. **102** (5), 10039–10054 (1997).
25. Smithsonian Volcanic Glass Data File. 2000 (http://www.nmnh.si.edu/minsci/research/glass/).
26. A. V. Sobolev and L. V. Dmitriev, "Primary Melts of Tholeiites of Oceanic Rifts (TOR): Evidence from Studies of Primitive Glasses and Melt Inclusions in Minerals," in *Proceedings of 28th International Geological Congress, Washington, USA* (Washington, DC, 1989), pp. 147–148.
27. A. V. Sobolev, Extended Abstract of Doctoral Dissertation in Geology and Mineralogy (GEOKhI RAN, Moscow, 1997).